Toward a Rational Design of Highly Folded Peptide Cation Conformations. 3D Gas-Phase Ion Structures and Ion Mobility Characterization

R. Pepin, K.J. Laszlo, A. Marek, B. Peng, M.F. Bush, Hélène Lavanant, Carlos Afonso, F. Tureček

HHS Public Access

Author manuscript

J Am Soc Mass Spectrom. Author manuscript; available in PMC 2016 October 01.

Published in final edited form as:

J Am Soc Mass Spectrom. 2016 October ; 27(10): 1647–1660. doi:10.1007/s13361-016-1437-6.

Toward a Rational Design of Highly Folded Peptide Cation Conformations. 3D Gas-Phase Ion Structures and Ion Mobility Characterization

Robert Pepin[1], **Kenneth J. Laszlo**[1], **Aleš Marek**[2], **Bo Peng**[1], **Matthew F. Bush**[1], **Helène Lavanant**[3], **Carlos Afonso**[3], and **František Tureček**[1]

[1]Department of Chemistry, Bagley Hall, University of Washington, Seattle, WA, USA

[2]Institute of Organic Chemistry and Biochemistry, Academy of Sciences of the Czech Republic, Prague, Czech Republic

[3]Laboratoire COBRA CNRS UMR 6014 & FR 3038, Université de Rouen, INSA de Rouen, Mont St Aignan Cedex, France

Abstract

Heptapeptide ions containing combinations of polar Lys, Arg, and Asp residues with non-polar Leu, Pro, Ala, and Gly residues were designed to study polar effects on gas-phase ion conformations. Doubly and triply charged ions were studied by ion mobility mass spectrometry and electron structure theory using correlated ab initio and density functional theory methods and found to exhibit tightly folded 3D structures in the gas phase. Manipulation of the basic residue positions in LKGPADR, LRGPADK, KLGPADR, and RLGPADK resulted in only minor changes in the ion collision cross sections in helium. Replacement of the Pro residue with Leu resulted in only marginally larger collision cross sections for the doubly and triply charged ions. Disruption of zwitterionic interactions in doubly charged ions was performed by converting the C-terminal and Asp carboxyl groups to methyl esters. This resulted in very minor changes in the collision cross sections of doubly charged ions and even slightly diminished collision cross sections in most triply charged ions. The experimental collision cross sections were related to those calculated for structures of lowest free energy ion conformers that were obtained by extensive search of the conformational space and fully optimized by density functional theory calculations. The predominant factors that affected ion structures and collision cross sections were due to attractive hydrogen bonding interactions and internal solvation of the charged groups that overcompensated their Coulomb repulsion. Structure features typically assigned to the Pro residue and zwitterionic COO-charged group interactions were only secondary in affecting the structures and collision cross sections of these gas-phase peptide ions.

Graphical abstract

Correspondence to: František Tureček; turecek@chem.washington.edu.

Electronic supplementary material The online version of this article (doi:10. 1007/s13361-016-1437-6) contains supplementary material, which is available to authorized users.

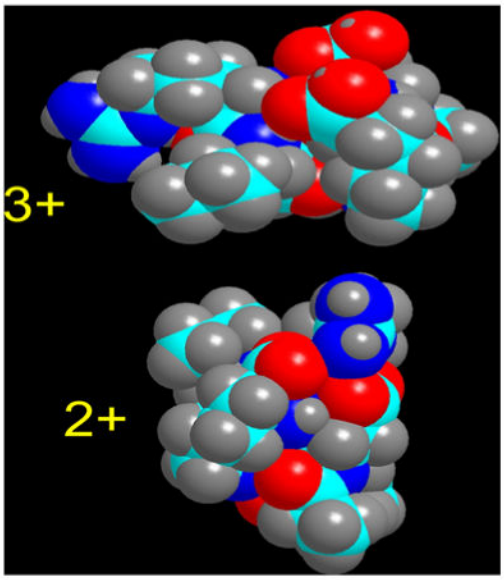

Keywords

Peptide ions; Ion mobility; Collisional cross sections; Density functional theory calculations; Ion structures; Polar effects

Introduction

Ionization and conversion of biomolecules from the condensed phase into the gas phase is associated with major changes in ion solvation, structure, and energetics. For example, amino acids that exist as stable zwitterions in aqueous solution at neutral pH prototropically rearrange to canonical forms upon evaporation [1–8] and ionization by proton [9–11] or metal ion attachment [12–21]. Electrospray ionization, which is commonly used to transport biomolecules from polar solution and convert them into gas-phase ions, may affect the biomolecule conformation to an extent that is difficult to predict. Several previous studies of gas-phase peptide ions generated by electrospray used ion mobility measurements that yielded collision cross sections that are sensitive to ion structure [22, 23]. Recent studies by Russell et al. showed that for some peptides, the ion conformers found in the gas phase depend on the electrospray solvent and interface temperature, leading to the formation of thermodynamically most stable conformers or those with “frozen” conformations pertinent to solution or electrospray droplets [24, 25]. Several gas-phase ions derived from natural [26–29] or modified peptides [30] have been found to correspond to the lowest free-energy conformers, as determined by a combination of collision cross sections from ion mobility measurements and vibrational band features from multiphoton infrared action spectroscopy. However, in general, the relationship between the conformations of peptides in solution and their gas-phase cations is not straightforward. For example, the amphipathic decapeptide GFLSILKKVL-NH_2, a fragment of the small protein melectin, was reported to prefer an α-helix conformation in solution [31], whereas gas-phase dications preferred globular structures for the lowest free-energy conformers [32]. An aggravating factor in the gas-phase

ion conformation studies is that the charge sites in the peptide ion are often unknown, and several tautomers must be considered for molecular modeling of ion structures.

Numerous peptides and miniproteins have been designed with the goal of having a particular well-defined local folding motif [33–36] or secondary structure in solution [37, 38]. An attempt has also been made to correlate the condensed phase 3D structure of a hydrophobic peptide from a transmembrane protein with the fragmentation of a gas-phase ion [39]. However, systematic studies aimed at dissecting the factors affecting gas-phase ion structures have been lacking.

Here, we report a study that combines experimental and computational analysis of gas-phase ion structures for a series of multifunctional heptapeptides, LKGXADR, LRGXADK, KLGXADR, and RLGXADK, which mainly form doubly and triply charged ions by electrospray. In these sequences, both the position and nature of the charge carrying Arg and Lys residues are permutated to allow for different modes of internal solvation of charged and polar neutral groups by hydrogen bonding. As the X residues, we use proline in a β-turn favoring GPAD motif [40–45] or the hydrophobic [46, 47] and β-turn disfavoring leucine [42]. The proline β-turn is associated with the C(O)- N_{Pro}-C_{α}-C(O) (ϕ) dihedral angle, which is fixed close to −65° because of the rigid pyrrolidine ring. Proline β-turns are common in various classes of β-hairpin motifs or loops found in many globular proteins [48]. In a related series of our model peptides, the carboxylic groups at aspartic acid residues and the C-termini were converted into methyl esters to block the formation of salt bridges in the lower charge states. Thus, the major polar interactions in these gas-phase ions can be modified by simple means and their effect on the ion conformation can be studied. Experimental collisional cross sections were obtained from drift-tube measurements [49]. Traveling-wave measurements [50, 51] have been used to obtain relative cross sections of ions from modified peptides. The experimental data are interpreted by comparing them with theoretical values that are based on structures that were fully optimized by density functional theory calculations. As in our previous peptide ion structure studies [26–30], we rely on using electron structure calculations, including electron correlation, to identify the lowest free-energy conformers and we probe if these are represented in the populations of gas-phase ions produced by electrospray ionization.

Experimental

Materials

Heptapeptides LKGPADR, LRGPADK, KLGPADR, and RLGPADK were purchased from United Biosystems (Cabin John, MD, USA) at 95% purity or better and used without further purification. Heptapeptides LKGLADR, LRGLADK, KLGLADR, and RLGLADK were purchased from Genscript (Piscataway, NJ, USA) at 95% purity or better and were used without further purification. Solvents and methylation reagents were purchased from Sigma Aldrich (St. Louis, MO, USA) and used as received. Heptapeptide methyl- and dimethyl esters were made by dissolving 1 equivalent peptide in anhydrous methanol containing 10 equivalents of HCl that was made by dissolving acetylchloride in anhydrous methanol. The tightly capped vial was left to react overnight at 40 °C. In some cases, the reaction mixture was left for a second night to increase conversion of the dimethyl ester products. Solvent

was evaporated and the resulting product was redissolved in electrospray solvent (MeOH:water:acetic acid, 50:50:1) to a concentration of ~10 μM. In some cases, this concentration was found to saturate the ion mobility detectors and a further dilution with water was performed.

Methods

Absolute ion mobilities in helium were measured on a Waters Synapt G2 HDMS (Manchester, UK) with a custom designed drift tube [49] in place of the standard traveling-wave ion mobility (TWIM) cell. Individual measurements concerned singly, doubly, and triply charged ions generated from individual parent peptides. The reported data are averages of 3–4 replicate measurements, each based on 6–10 field-dependent arrival times with a linearity coefficient $r^2 \geq 0.999$. Relative ion mobility drift times were acquired on a Waters Synapt G2 using the TWIM methodology with nitrogen as the mobility gas. In each case, ion mobilities were measured for a mixture of the peptide and its methyl esters to ensure the ion arrival times were obtained under identical experimental conditions for all components and charge states. The wave velocities in the TWIM measurements were 300, 315, and 350 m/s and the experimental arrival times were corrected according to a procedure reported by Ruotolo et al [52, 53].

Calculations

Peptide ion structures were generated using the ConformSearch engine described previously [27, 29]. Briefly, this consists of (1) selection of starting structures for protonated ion tautomers; (2) molecular dynamics trajectory calculations run at eight temperatures (300, 345, 397, 457, 525, 604, 695, and 800 K) using the CHARMM force field [54] and a replica exchange protocol [55] to generate 800,000 conformer structures for each peptide ion tautomer; (3) sampling 8000 structures for full geometry optimization with the semi-empirical PM6 method [56]; (4) sorting out conformer families according to their hydrogen bonding patterns, and compacting duplicates; (5) density-functional theory (DFT) single-point energy calculations with the hybrid B3LYP [57, 58] functional and the 6-31+G(d,p) basis set on ca. 120–200 lowest energy conformers in each family; (6) resorting the conformers according to B3LYP single-point energies; (7) full gradient geometry optimization with B3LYP and M06-2X [59]/6-31+G(d,p) of 30–40 lowest-energy conformers; (8) harmonic frequency calculations of 10–20 lowest energy conformers, and (9) single-point-energy calculations with B3LYP, M06-2X, and Møller-Plesset perturbational theory [60] truncated at second order with valence-electron only excitations [MP2(frozen core)], all with the 6-311+G(2d,p) basis set. Select ion structures were reoptimized with ωB97X-D [61] DFT calculations employing the 6-31+G(d,p) basis set, and used for ωB97X-D/6-311+G(2d,p) single-point energy calculations. All electronic structure calculations were performed with the Gaussian 09 suite of programs [62]. The optimized ion geometries of select structures in the Cartesian coordinate format are in Supplementary Tables S1–S20 (Supporting Material). The other structures can be obtained from the corresponding author upon request. Atomic charges were calculated as Mulliken populations [63] and with the natural population analysis [64] and Singh-Kollman [65] schemes. Dipole moments were calculated in a field-independent coordinate system.

Collisional cross sections pertinent to fully optimized ion conformer structures and B3LYP/6-311+G(2d,p) atomic charges were calculated using the Mobcal program [66, 67] with the parameters set by Campuzano et al. [68]. Comparisons between the parameters optimized for drug-like molecules in Campuzano et al.'s work with the default parameters were made and found to produce no significant differences for our results. The use of atomic charge densities calculated with the Singh-Kollman scheme [65], as recommended by Campuzano et al. [68, 69] resulted in negligible (<0.7%) changes in the calculated cross sections.

Results

Ion Mobility Measurements

Ion mobility measurements of ions derived from the four basic heptapeptides, KLGPADR, LKGPADR, LRGPADK, and RLGPADK, were carried out in helium and the obtained absolute collisional cross sections (Ω_{abs}) are summarized in Table 1. The arrival time peaks for the parent doubly and triply charged ions showed single Gaussian-like intensity profiles (Figure 1), indicating the presence of one conformer or a mixture of conformers of very similar Ω_{abs}. The data showed a general trend of Ω_{abs} increasing with the ion charge [70]. The Ω_{abs} dependence on the peptide sequence showed different results for different charge states. Starting with triply charged ions, the order of Ω_{abs} was LRGPADK < LKGPADR < RLGPADK ≅ KLGPADR, showing slightly greater Ω_{abs} for peptide ions having the charge-carrying polar residues at the *N*-terminus. This order changed for doubly charged ions where it was RLGPADK ≤ LRGPADK < KLGPADR < LKGPADR with a very small effect of the *N*-terminal R or L and a small change when the *N*-terminal L and K were swapped. Overall, the sequence variations resulted in 8% and 5.4% changes in the Ω_{abs} for the triply and doubly charged ions, respectively.

The Ω_{abs} for the present set of doubly charged ions were compared with the data in the extensive set of peptides reported by Clemmer et al. [71]. The Ω_{abs} show an increasing trend with the ion mass [71] and thus a subset of 25 doubly charged tryptic heptapeptides comparable to our ions were used for comparison. The Ω_{abs} from the Clemmer tryptic heptapeptide subset showed the tightest correlation with the total number of atoms in the ion (N)[72], $\Omega_{abs} = 1.442N + 39.55$, giving a correlation coefficient $r^2 = 0.837$, and standard deviation $s = 4.9$ Å^2 (Supplementary Figure S1, in Supporting Material). The Ω_{abs} for $LKGPADR^{2+}$ falls very close to the fit line and that for $LKGPADR^{2+}$ is one standard deviation lower. The Ω_{abs} for $LRGPADK^{2+}$ and $RLGPADK^{2+}$ are more than one s lower, qualifying these peptides as having tightly folded structures relative to the tryptic heptapeptide set.

Ion mobility measurements of the heptapeptide library as well as the dimethyl ester analogs were carried out on a Waters Synapt G2 using the TWIMS technology [51] and nitrogen as the collision gas (Table 2). TWIMS provides an efficient means for rapid screening of arrival times in a mass-resolved mixture. It provides relative drift times, t_d, which imply the *relative* gas-phase sizes of various analyte ions but do not give absolute cross sections. The Ω correlate with the t_d according to the formula $\Omega = a t_d^n$ where n is close to 0.5 [68]. For small differences in the t_d (<5%) the derived Ω scale approximately linearly with t_d. Hence, the *relative* arrival times ($t_{d,rel}$) can be used as a measure of *relative* Ω for the investigations of

the effect on the molecular shape of modifications in the amino acid residue (L versus P) and polar groups where the acidic carboxyl groups are converted to neutral methyl ester groups.

Replacing proline with leucine in all doubly and triply charged ions resulted in a very minor increase of the $t_{d,rel}$ ranging from 1% to 4%, which was comparable to the typical reproducibility of these measurements [73]. This may indicate that the proline β-turn affects the shape of these peptide ions to only a small extent. Accordingly, the charge-dependent increase of the $t_{d,rel}$ upon adding a third charge to the leucine-containing ions (18%–20%) was similar to that observed for the proline peptide ion series (13%–25%). The differences between the Pro and Leu containing doubly and triply charged ions are substantially smaller than what would be expected on the basis of the estimated amino acid size parameters for singly charged ions with 5–10 residues that predict 15%–19% larger cross sections for Leu peptides [71, 72, 74].

An interesting observation followed from comparing the $t_{d,rel}$ of the parent carboxyl-containing peptide ions with those of their dimethyl esters (Table 2). For most triply charged ions, the dimethyl esters showed marginally *smaller* $t_{d,rel}$ than the corresponding carboxylic peptide ions. The RLGPADK system was an exception, where both the doubly and triply charged dimethyl ester showed an increase in the $t_{d,rel}$ relative to the corresponding carboxylic peptide ions. The other doubly charged ions showed only small relative t_d variations, both positive and negative, resulting from esterification.

Calculated Ion Structures

To relate the experimental Ω to ion structures, we calculated the theoretical cross sections for families of lowest free-energy conformers of the peptide ions, the structures of which were produced by multi-step DFT and ab initio calculations. In general terms, the triply charged ions carry the protons on the three basic groups, which are the *N*-terminal and Lys side-chain amines and the Arg guanidine group. Hence, there is only one tautomer for each triply charged ion. The optimized structures of triply charged LKGPADR, KLGPADR, and RLGPADK ions pointed to specific conformations for the lowest free-energy ions. The relative free energies at 298 K for the most stable conformers are summarized in Table 3. The lowest free-energy $LKGPADR^{3+}$ conformer **1** (Figure 2) displayed four hydrogen bonds from the charged groups, out of which three were for Lys and one for Arg, and one neutral H bond for the Asp carboxyl. Hydrogen bonds of the X—H…Y type were assigned according to the IUPAC definition [75]. The charged *N*-terminal amino group was extended out and internally solvated by a single hydrogen bond to the Leu amide. A similar H-bonding pattern was found for conformer **2**, which had 12–14 kJ mol^{-1} higher free energy than **1** at 298 K. The chief difference between these low-energy conformers was in the ψ_6 dihedral angle at the Asp residue as a result of rotation of the C-terminal Arg residue (Figure 2). This is also characterized by different distribution of atomic charges, resulting in different dipole moments for **1** and **2** (Table 3). A notable feature of these low-energy structures is the wide-open hinge at the Pro residue, which is enforced by the strong hydrogen bond of the Lys ε-ammonium to the Ala amide carbonyl (Figure 2). It is noteworthy that these low-energy ion structures lack any H-bonds of the 4→1 type between the Gly carbonyl and the Asp NH that would indicate a β-turn motif [40, 42].

The lowest free-energy KLGPADR^{3+} conformers **3**–**5** showed different H-bonding patterns (Figure 3). In the KLGPADR^{3+} conformer **3**, each of the charged *N*-terminal and Lys ammonium groups was internally solvated by forming two hydrogen bonds, whereas the Arg charged group had only one H-bond to the Asp amide. The hydrogen bonding of the *N*-terminal ammonium group forced the backbone to make a loop with hinges at the Leu and Pro residues. This conformer had the largest dipole moment of all these triply-charged ions. A similar pattern was found for the lower-energy conformer **4** where the backbone loop was strengthened by another H-bond of the *N*-terminal ammonium to the Asp carboxyl group. Structures **3** and **4** mainly differ in the orientation of the Arg residue, which is caused by different ψ_5 torsional angles at Asp. In contrast, the *N*-terminal ammonium group in another conformer **5** was extended out and internally solvated by a single H-bond to the Lys amide. This weaker solvation of the *N*-terminal ammonium was compensated by tri-coordination of the Lys ε-ammonium to the Gly and Ala amides and the C-terminal carboxyl that formed a side-chain loop affecting the peptide ion structure. The ion conformation was further shaped by a neutral H-bond of the C-terminal carboxyl to the Leu amide that formed a macrocyclic ring structure with hinges at Ala and Asp that was capped by the Lys ε-ammonium group. Another energetically favorable feature of **5** was the double H-bond solvation of the Arg charged group by the Asp amide and carboxyl groups. The efficient internal solvation of the charged groups in these ions obliterates neutral H-bonding between the Gly and Asp residues that would be expected for a β-turn folding motif [40, 42].

The RLGPADK^{3+} ions showed different folding patterns in low free-energy conformers that differed in side-chain conformations and internal solvation of the charged groups (Figure 4). In one group of conformers, represented by structure **6**, the Arg charged side chain group was internally solvated by a single H bond to the Arg amide, the *N*-terminal ammonium formed H-bonds to the Asp amide and carboxyl and Gly amide, and the Lys ammonium was solvated by the Leu, Pro, and Ala amides. Interestingly, another low-energy conformer (**7**, Supplementary Figure S2) had an unfolded Arg side chain so the charged guanidinium group lacked internal solvation. In another major group (**8** and **9**), the Arg charged side chain group was internally solvated by the Asp side-chain carboxyl, the *N*-terminal ammonium formed H-bonds to the Asp amide and the C-terminal carboxyl, and the Lys ammonium was solvated by the Gly, Pro, and Ala amide carbonyls. In **10** and **11**, the Arg side chain was H bonded to the Leu amide, the *N*-terminal ammonium formed H-bonds to the Asp amide and the C-terminal carboxyl, and the Lys charged group was hydrogen bonded to the Pro and Gly or Ala amide carbonyls. Hydrogen bonding of the Gly residue to the charged groups in **6**, **7**, **9**–**11**, prevents the formation of a regular β-turn in these peptide ions. The different conformations and arrangements of atomic charges in these triply charged peptide ions result in a rather broad (5–22 D) range of dipole moments.

Methylation of both carboxyl groups in RLGPADK^{3+} affected the conformer relative energies. The methyl esters derived from **6** and **7** showed quite comparable energies, whereas that from the more stable conformer **8** was substantially less stable (Supplementary Figure S3). These changes in relative energies are associated with the hydrogen bonding patterns in the ions. In **6** and **7**, the hydrogen bonding does not involve the carboxyl protons, and the strong *N*-terminal and Lys ammonium hydrogen bonding is preserved in the

dimethyl esters to maintain the backbone loop with hinges at the Pro and Ala residues (Supplementary Figure S3). In contrast, carboxyl methylation in **8** disrupts the very strong hydrogen bond between the Asp carboxyl and the Leu amide carbonyl, which also affects the other hydrogen bonds in the methyl ester and alters the ion conformation.

Doubly Charged Ions

In contrast to the triply charged ions, the doubly charged ions allowed for the formation of three canonical and two zwitterionic tautomers from each peptide sequence, leading to 20 groups of conformers. Considering the substantial computational demands of the multi-step conformational analysis at the ConformSearch level of theory, addressing all 20 ion tautomers would be a daunting task. Therefore, we selected a limited number of doubly charged tautomers for each peptide sequence for extensive structure analysis. The relative free energies for the most stable conformers are shown in Table 4.

Starting with $LRGPADK^{2+}$, extensive conformational search was performed for Asp and C-terminal carboxylate zwitterionic tautomers with an initial *trans* Gly-Pro amide configuration. A separate search starting from a *cis* Gly-Pro amide configuration resulted in *cis*-*trans* amide rotation to chiefly yield *trans* Gly-Pro conformers. The *cis* isomers that reached full geometry optimization were in general less stable than the low-energy *trans* isomers. The two lowest free-energy Asp-zwitterions (**12**, Figure 5, and **13**, Supplementary Figure S2) showed multiple H-bonds, providing internal solvation to the charged groups. In both ions, the Asp carboxylate was internally solvated by the Arg and Lys charged groups whereas the *N*-terminal ammonium was remote and received internal solvation through H-bonding to the Pro and Ala amides. In the lowest free energy C-terminal zwitterion (**14**, Figure 5), the carboxylate participated in H-bonding to the Arg and *N*-terminal charged groups, whereas the Lys ammonium developed three H-bonds to the Gly, Pro, and Asp amides. It is worth noting that the C-terminal zwitterion **14** was thermochemically less stable than **12** and **13** but had a higher entropy, which contributed to its low free energy. The different folding patterns in **12**, **13**, **14**, and related conformers **15** and **16** (Supplementary Figure S2) had only very minor effects on the collision cross sections in these ions, as discussed in detail below.

Swapping the Lys and Arg residues in LRGPADK resulted in $LKGPADR^{2+}$ ions that were generated as Asp carboxylate zwitterions. The lowest free energy structures for these tautomers **17**–**20** showed a conserved folding pattern, which is represented by structure **17** (Figure 5), and the others are shown in Supplementary Figure S4. In conformer **17**, the Asp carboxylate was positioned on the top of a highly folded structure, where it was internally solvated by H-bonds from the Lys and *N*-terminal ammonium groups and a strong H-bond from the Leu amide. The Arg charged group was internally solvated by the Pro, Gly, and Lys amide carbonyls. The ion conformation was further locked in by a H-bond between the Lys ammonium and the C-terminal carboxyl group.

Swapping the Leu and Lys residues in LKGPADR formed $KLGPADR^{2+}$ ions. Upon molecular dynamics and full geometry optimization, a number of Asp-zwitterionic structures converged to a family of lowest free-energy conformers **21**–**24**, the folding pattern of which is represented by **21** (Figure 5). The other conformers are shown in Supplementary Figure

S4. Conformer **21** had the Asp carboxylate internally solvated by H-bonds to the Lys and *N*-terminal ammonium groups. The charged Arg group was remote from the carboxylate, but cooperatively interacted by forming a strong H-bond to the Asp carbonyl. This interaction polarized the Asp amide N–H bond to strengthen the H-bond to the Asp carboxylate. A salient feature of these ions was that the Lys charged group formed only a single H-bond, whereas the protons of the *N*-terminal ammonium were fully internally solvated by the Lys and Gly amides in addition to the Asp carboxylate. Moving the Lys ammonium proton in **21** to the Asp carboxylate resulted in a canonical structure that was a local energy minimum (**24**, Supplementary Figure S5) when optimized by B3LYP and M062X. However, optimization with ωB97XD resulted in a spontaneous reverse proton migration forming **21**. The **21** → **24** proton transfer indicated by B3LYP and M062X calculations was nearly thermoneutral and did not alter the overall folding pattern of the ion. Note the very short distance between the COOH proton and the Lys ε-amine nitrogen in **24** (1.466 Å) and the similarly short N-H…OCO distance in **21** (1.519 Å), which are indicative of the fluxional nature and highly anharmonic N–H and O–H stretching vibrational modes in these tautomers [28, 76]. In contrast to **24**, moving a proton from the *N*-terminal ammonium to the Asp carboxylate did not result in a local energy minimum and the structure spontaneously collapsed back to **21**.

The lowest free-energy conformers of the last sequence, $RLGPADK^{2+}$, were found to prefer a folding pattern, which is represented by conformer **25** (Figure 5). This Asp-zwitterion had the carboxylate internally solvated by the charged Arg and *N*-terminal ammonium groups and the neutral C-terminal carboxyl. All three protons of the Lys ε-ammonium were internally solvated by forming H bonds to the Pro, Gly, and Leu amide carbonyls. The related conformers **27** and **26** (Supplementary Figure S6) had free energies very close to that for **25** and may coexist with it under equilibrium conditions in the gas phase.

Discussion

Relative Energies of Sequence Isomers

The conformer relative energies can be related to the combination of major noncovalent electrostatic interactions in the ions that can be expressed as a sum of attractive ion–dipole ($E_{id} < 0$) and repulsive pair-wise Coulomb ($E_c > 0$) interactions of the charged groups. The calculated DFT relative energies include contributions from all these interactions and thus allow one to gauge the relative ion–dipole interactions in a semiquantitative manner and relate them to the major structure features in the optimized structures. The effects of Coulomb interactions on the thermochemistry of multiply charged ions have been addressed previously for non-peptidic [77–79] as well as peptide ions [80, 81]. The pairwise Coulomb energies were estimated from the standard formula, $E_c(\text{kJ mol}^{-1}) = \Sigma 1389.38/R_{ij}$, where the distance ($R_{ij}$ in Å) between the charged groups *i* and *j* was measured from the central atoms (N for ammonium and C for guanidinium). For example, the thus estimated Coulomb energy in **1** (362 kJ mol^{-1}) was 15 kJ mol^{-1} higher than that in **2** (347 kJ mol^{-1}), yet the former conformer was 10–14 kJ mol^{-1} more stable. This implied that the attractive ion–dipole interactions contributed to ca. 25–30 kJ mol^{-1} greater stabilization in **1** compared to those in

2. The optimized ion structures (Figure 2) indeed showed slightly tighter H-bonds of the charged groups in **1** compared with those in **2**.

With $KLGPADR^{3+}$ ions, the charged groups in conformers **3** and **4** had relatively high Coulomb energy (480 and 498 kJ mol^{-1}, respectively) compared with that in **5** (469 kJ mol^{-1}). This is in part reflected by the B3LYP and ωB97X-D relative energies that placed **5** as the lowest energy conformer, whereas M06-2X placed it above **3** and **4** (Table 3). Note that conformers **3** and **4** had quite different hydrogen bonding patterns than **5** so that their different ion–dipole interactions could not be readily assigned to the strength of particular hydrogen bonds.

Amongst the $RLGPADK^{3+}$ conformers, the lowest energy structure **8** showed the highest Coulomb repulsion energy (565 kJ mol^{-1}), underscoring the dominant effect of ion–dipole stabilization of the ion. Structures **6** and **10**, which had notably lower Coulomb energies (498 and 488 kJ mol^{-1}, respectively) were less stable than **8**. Hence, the DFT energy data indicate that considering the Coulomb energy alone may be unreliable for assessing ion conformer relative stabilities, and a careful analysis of all interactions, preferably through electron structure calculations, is recommended.

It is worth noting that the DFT relative energies diverged for B3LYP and M06-2X in assigning the lowest energy conformers for some peptide sequences. For example, B3LYP energies pointed to **11** as the lowest-energy $RLGPADK^{3+}$ conformer, whereas M06-2X calculations preferred **8** (Table 3). This resulted in a 23 kJ mol^{-1} divergence in the relative energies between these conformers. A similar divergence was found for **3** and **5**, where the latter was the lowest energy structure by B3LYP and MP2, but 6 kJ mol^{-1} less stable than **4** by M06-2X. Divergence of this magnitude for relative energies of some peptide ions has been observed previously for calculations that used different ab initio and DFT methods [27, 82]. The nature of this effect is not well understood, although the differences are within the expected accuracy confidence limits of DFT calculations [58, 59, 61]. Calculations of other peptide ions (e.g., $LKGPADR^{3+}$) showed consensus in the order of relative energies obtained by MP2 and three DFT methods. We addressed this issue by examining the energies of the contentious conformers by single-point calculations with another hybrid functional that includes dispersion interactions, which is ωB97X-D [61] using B3LYP, M06-2X, and ωB97X-D fully optimized geometries. The goal was to probe if small differences in the respective geometry parameters had an effect on the relative energies. The ωB97X-D calculations gave absolute energies that were overall ca. 0.08 atomic units (1 a.u. = 2625.5 kJ mol^{-1}) lower for the M06-2X optimized structures than for the B3LYP ones because of a better fit of bond lengths between the ωB97X-D and M06-2X optimized structures. However, the trends in the ωB97X-D single-point relative energies were the same regardless of the underlying optimized geometry. Thus, for $KLGPADR^{3+}$ the ωB97X-D calculated energies agreed with those from B3LYP and MP2 in preferring conformer **5** as the lowest energy structure, although by a smaller margin than the other methods (Table 3). The calculated relative free energies were used to obtain the pairwise equilibrium constants at 298 K, using the standard formula, $-\Delta G_T = RT\ln K_{eq}$, and to estimate the conformer molar fractions. When based on the ωB97X-D energies, these indicated a 18/81 mixture of **4** and **5**, with **3** being a minor (0.9%) component. In contrast, ωB97X-D energies for $RLGPADK^{3+}$

agreed with those from M06-2X in preferring **8** as the lowest energy conformer and predicting its molar fraction as being close to 98% at 298 K. These results indicate that multiple DFT and ab initio methods should be used to assess the ordering of peptide ion relative energies. Structures for which the methods disagree are problematic and might require additional calculations, although at this point it is not clear which methods can provide most reliable relative energies for gas-phase peptide ions.

Correlation Between the Calculated and Ion Mobility Collision Cross Sections

The energy calculations identified the lowest free-energy conformers for the gas-phase peptide ions. We now compare the collision cross sections that were calculated for the lowest free-energy conformers (Ω_{th}) with the experimental data (Ω_{abs}). The calculations were based on both B3LYP and M06-2X fully optimized structures that showed minor variations in bond lengths, angles, and dihedral angles for each ion conformer. Collision cross section calculations were run with three different models, which were the projection average approximation (PA)[83, 84], elastic-hard-sphere scattering (EHSS)[66, 85], and ion trajectory model (TM)[86, 87], which is also available with a modified set of parameters (TM_{opt}) [68]. In general, these models give different Ω_{th} for the same geometry and charge distribution in the peptide ion, following the trend $\Omega(PA) < \Omega(TM_{opt}) < \Omega(TM) < \Omega(EHSS)$ for both the doubly and triply charged heptapeptide ions. Hence, the conversion into Ω_{th} of the ab initio or DFT-calculated molecular parameters depends on the computational method, which is further underscored by the differences in the optimized ion geometries generated by different density functionals. On the basis of our previous studies of singly and doubly charged peptide ion conformers [27–30], we considered all combinations of B3LYP and M06-2X structures with PA, EHSS, and TM methods, as given in Supplementary Tables S1 and S2 for the doubly and triply charged ions, respectively. To evaluate the overall accuracy of the calculated data, we show the deviations of the calculated Ω_{th} from the Ω_{abs} (Figure 6) and discuss the Ω_{th} calculated with the ion trajectory methods.

The triply charged ions showed different degrees of agreement between the Ω_{th} and Ω_{abs} (Figure 6a, b). The Ω_{th} for the low free-energy $LKGPADR^{3+}$ conformers **1** and **2** were slightly higher than the Ω_{abs}, in particular for the B3LYP optimized structures (Figure 6a), but the agreement improved to within 4% for the M06-2X structures (Figure 6b). In contrast, the Ω_{th} for all low free-energy $KLGPADR^{3+}$ (**3**–**5**) and especially $RLGPADK^{3+}$ conformers **6**–**11** were substantially lower than the Ω_{abs} with deviations for the ion trajectory methods approaching or even exceeding 10%. The reason for this discrepancy is not obvious because the structures, energies, and Ω_{th} for all these peptide ions were treated at the same level of theory. At the same time, the calculated dipole moments for the conformers show only negligible effects on the Ω_{th}, perhaps because of the low polarizability of the helium collision gas. It is possible that the $KLGPADR^{3+}$ and $RLGPADK^{3+}$ ions produced by electrospray assume higher free-energy, more expanded conformations as a result of being frozen in non-equilibrium populations upon transition to the gas phase [24, 25].

Regarding the doubly charged ions, the $LRGPADK^{2+}$ conformers **12**–**16** showed agreement within 5% between the experimental Ω_{abs} and the Ω_{th} obtained by ion trajectory calculations for conformers **13** and **15** (Figure 6c, d). Note that these are not the lowest free-energy

conformers (Table 4). The match was even closer (<3%) for the M06-2X optimized structures, which are often more compact than the B3LYP ones [27], and included the lowest-free energy conformers **12** and **16** (Figure 6d). Hence, the closest match between the Ω_{abs} and Ω_{th} depends on the computational method used, and care should be taken to use it for unambiguous structure assignment. A close match was obtained for $LKGPADR^{2+}$ and $RLGPADK^{2+}$ where the Ω_{abs} and ion trajectory Ω_{th} were within 5% for the low-energy conformers (Figure 6c, d). The calculated relative free energies for the thermodynamically most stable $LKGPADR^{2+}$ and $RLGPADK^{2+}$ conformers are very similar (Table 4), indicating that peptide ions with these sequences may exist in equilibrium mixtures that are not resolved by ion mobility measurements. The Ω_{th} for $KLGPADR^{2+}$ showed less satisfactory agreement as they were >7% greater than Ω_{abs} when based on M06-2X optimized structures (Figure 6d), and even larger when based on B3LYP structures (Figure 6c).

Replacing the Pro residue with Leu had only a very small effect on the collision cross sections of all doubly and triply charged ions. We addressed this topic with the $RLGXADK^{3+}$ system for which we obtained optimized ion structures **8** and its Leu homologue **8**-Leu (Supplementary Figure S7). These structures illustrated that there were only minor changes in the backbone and charged-group conformation upon replacing Pro with Leu, as evidenced by the nearly identical hydrogen bonds of the Lys side chain and *N*-terminal ammonium groups, and the Arg guanidinium group. These charge-solvating interactions, together with the strong H-bonding of the Asp carboxyl to the Leu-2 amide, were the major factors defining the ion overall conformation and collision cross section. The calculated Ω_{th} for **8** and **8**-Leu showed 4.4%–5.5% increase upon replacing Pro with Leu to be compared with a 1% increase when based on the $t_{d,rel}$. Given the combined uncertainties in both types of values, this represents an acceptable agreement.

The effect on the Ω of converting the peptide ions into their methyl esters was computationally studied for $RLGPADK^{3+}$ only. In this case, the dimethyl ester conformers were not sorted out by extensive search of their conformational space and so the comparison is limited. The Ω_{th} for the dimethyl ester showed 2%–3% increase compared with that for the $RLGPADK^{3+}$ conformer **8**. This is in only a qualitative agreement with the trend in the $t_{d,rel}$, which indicated a larger (28%) increase upon methylation. Despite the approximate quantitation of the Ω_{th} in this case, this computational result is consistent with the respective $t_{d,rel}$ for the majority of peptide ions where only minor changes in arrival times were observed between the free doubly and triply charged peptides and their dimethyl esters. One should consider that the accuracy of absolute cross section measurements is currently estimated at ± 3% in the literature [53], and most of the sequences show differences between the native and ester forms within this margin.

Conclusions

Analysis of experimental collision cross sections (Ω) for multiple charge states of several heptapeptide ions containing polar basic and acidic residues indicates consistent effects of the ion charge. In contrast, structure modifications, such as replacing Pro with Leu and converting Asp and C-terminal carboxylates to methyl esters, had only minor effects on the

experimental Ω. Electron structure calculations in combination with extensive searches of the conformational space identified low free-energy structures for the peptide ions. These showed tightly folded conformations in which internal solvation of the charged groups overcompensated their Coulomb repulsion. Specific neutral hydrogen bonds, such as those imposing β-turns in proline containing peptides, were found to be unimportant in these gas-phase ions. Comparison of calculated and experimental Ω showed dependence on the theoretical model. The differences between the calculated Ω for these peptide ion conformers were too small to allow structure assignment to be made on ion mobility measurements alone.

Supplementary Material

Refer to Web version on PubMed Central for supplementary material.

Acknowledgments

Support by the Chemistry Division of the National Science Foundation (Grant CHE-1359810 to F.T.) is gratefully acknowledged. M.F.B. thanks the American Society for Mass Spectrometry, the NIGMS (Award Number T32GM008268), and the ARCS Foundation for support. Research at Universite de Rouen has been supported by the European Regional Development Fund (ERDF) N°31708, and Labex SynOrg (ANR-11-LABX-0029).

References

1. Locke MJ, McIver RT Jr. Effect of solvation on the acid/base properties of glycine. J Am Chem Soc. 1983; 105:4226–4232.
2. Suenham RD, Lovas FJ. Millimeter wave spectrum of glycine. J Mol Spectrosc. 1978; 72:372–382.
3. Brown RD, Godfrey PD, Storey JWV, Bassez M-P. Microwave spectrum and conformation of glycine. J Chem Soc Chem Commun. 1978:547–548.
4. Iijima K, Tanaka K, Onuma S. Main conformer of gaseous glycine: molecular structure and rotational barrier from electron diffraction data and rotational constants. J Mol Struct. 1991; 246:257–266.
5. Lovas FJ, Kawashima Y, Grabow JU, Suenram RD, Fraser GT, Hirota E. Microwave spectra, hyperfine structure, and electric dipole moments for conformers I and II of glycine. Astrophys J. 1995; 455:L201–L204.
6. Linder R, Nispel M, Haeber T, Kleinermanns K. Gas-phase FT-IR-spectra of natural amino acids. Chem Phys Lett. 2005; 409:260–264.
7. de Vries MS, Hobza P. Gas-phase spectroscopy of biomolecular building blocks. Ann Rev Phys Chem. 2007; 58:585–612. [PubMed: 17291183]
8. Linder R, Seefeld K, Vavra A, Kleinermanns K. Gas phase infrared spectra of nonaromatic amino acids. Chem Phys Lett. 2008; 453:1–6.
9. Clemmer DE, Jarrold MF. Ion mobility measurements and their applications to clusters and biomolecules. J Mass Spectrom. 1997; 32:577–592.
10. Wyttenbach T, Witt M, Bowers MT. On the stability of amino acid zwitterions in the gas phase. The influence of derivatization, proton affinity, and alkali ion addition. J Am Chem Soc. 2000; 122:3458–3464.
11. Wu R, McMahon TB. Stabilization of zwitterionic structures of amino acids (Gly, Ala, Val, Leu, Ile, Ser, and Pro) by ammonium ions in the gas phase. J Am Chem Soc. 2008; 130:3065–3078. [PubMed: 18271581]
12. Bush MF, Forbes MW, Jockusch RA, Oomens J, Polfer NC, Saykally RJ, Williams ER. Infrared spectroscopy of cationized lysine and ε-N-methyllysine in the gas phase: effects of alkali-metal ion size and proton affinity on zwitterion stability. J Phys Chem A. 2007; 111:7753–7760. [PubMed: 17636967]

13. Julian RR, Jarrold MF. Gas-phase zwitterions in the absence of a net charge. J Phys Chem A. 2004; 108:10861–10864.
14. Lemoff AS, Bush MF, Williams ER. Binding energies of water to sodiated valine and structural isomers in the gas phase: the effect of proton affinity on zwitterion stability. J Am Chem Soc. 2003; 125:13576–13584. [PubMed: 14583055]
15. Cerda BA, Wesdemiotis C. Zwitterionic versus charge-solvated structures in the binding of arginine to alkali metal ions in the gas phase. Analyst. 2000; 125:657–660.
16. Dunbar RC, Polfer NC, Oomens J. Gas-phase zwitterion stabilization by a metal dication. J Am Chem Soc. 2007; 129:14562–14563. [PubMed: 17985905]
17. Bush MF, Oomens J, Saykally RJ, Williams ER. Alkali metal ion binding to glutamine and glutamine derivatives investigated by infrared action spectroscopy and theory. J Phys Chem A. 2008; 112:8578–8584. [PubMed: 18714968]
18. Bush MF, Oomens J, Williams ER. Proton affinity and zwitterion stability: new results from infrared spectroscopy and theory of cationized lysine and analogues in the gas phase. J Phys Chem A. 2009; 113:431–438. [PubMed: 19128186]
19. Prell JS, O'Brien JT, Steill JD, Oomens J, Williams ER. Structures of protonated dipeptides: the role of arginine in stabilizing salt bridges. J Am Chem Soc. 2009; 131:11442–11449. [PubMed: 19624125]
20. Drayss MK, Armentrout PB, Oomens J, Schaefer M. IR spectroscopy of cationized aliphatic amino acids: stability of charge-solvated structure increases with metal cation size. Int J Mass Spectrom. 2010; 297:18–27.
21. Pathak AK. Stabilizing the zwitterionic form of amino acids in the gas phase: an ab initio study on the minimum number of solvents and ions. Chem Phys Lett. 2014; 610/611:345–350.
22. Gill AC, Jennings KR, Wyttenbach T, Bowers MT. Conformations of biopolymers in the gas phase: a new mass spectrometric method. Int J Mass Spectrom. 2000; 195/196:685–697.
23. Shelimov KB, Clemmer DE, Hodgins RR, Jarrold MF. Protein structure in vacuo: gas-phase conformations of BPTI and cytochrome *c*. J Am Chem Soc. 1997; 119:2240–2248.
24. Fort KL, Silveira JA, Pierson NA, Servage KA, Clemmer DE, Russell DH. From solution to the gas phase: factors that influence kinetic trapping of Substance P in the gas phase. J Phys Chem B. 2014; 118:14336–14344. [PubMed: 25402008]
25. Silveira JA, Fort KL, Kim D, Servage KA, Pierson NA, Clemmer DE, Russell DH. From solution to the gas phase: stepwise dehydration and kinetic trapping of Substance P reveals the origin of peptide conformations. J Am Chem Soc. 2013; 135:19147–19153. [PubMed: 24313458]
26. Tureček F, Chung TW, Moss CL, Wyer JA, Ehlerding A, Holm AIS, Zettergren H, Nielsen SB, Hvelplund P, Chamot-Rooke J, Bythell B, Paizs B. The histidine effect. Electron transfer and capture cause different dissociations and rearrangements of histidine peptide cation-radicals. J Am Chem Soc. 2010; 132:10728–10740. [PubMed: 20681705]
27. Moss CL, Chamot-Rooke J, Brown J, Campuzano I, Richardson K, Williams J, Bush M, Bythell B, Paizs B, Tureček F. Assigning structures to gas-phase peptide cations and cation-radicals. An infrared multiphoton dissociation, ion mobility, electron transfer and computational study of a histidine peptide ion. J Phys Chem B. 2012; 116:3445–3456. [PubMed: 22364440]
28. Tureček F, Moss CL, Pikalov I, Pepin R, Golyuz K, Polfer NC, Bush MF, Brown J, Richardson K. Gas-phase structures of phospho-peptide ions: a difficult case. Int J Mass Spectrom. 2013; 354/355:249–256.
29. Pepin R, Laszlo KJ, Peng B, Marek A, Bush MF, Tureček F. Comprehensive analysis of Gly-Leu-Gly-Gly-Lys peptide dication structures and cation-radical dissociations following electron transfer: from electron attachment to backbone cleavage, ion-molecule complexes and fragment separation. J Phys Chem A. 2014; 118:308–324. [PubMed: 24328203]
30. Marek A, Pepin R, Peng B, Laszlo KJ, Bush MF, Tureček F. Electron transfer dissociation of photolabeled peptides. Backbone cleavages compete with diazirine ring rearrangements. J Am Soc Mass Spectrom. 2013; 24:1641–1653. [PubMed: 23633016]
31. Čeřovský V, Hovorka O, Cvačka J, Voburka Z, Bednářová L, Borovičková L, Slaninová J, Fučík V. Melectin: a novel antimicrobial peptide from the venom of the cleptoparasitic bee *Melecta albifrons*. Chem BioChem. 2008; 9:2815–2821.

32. Moss CL, Chung TW, Čeřovský V, Tureček F. Electron transfer dissociation of a melectin peptide: correlating the precursor ion structure with peptide backbone dissociations. Coll Czech Chem Commun. 2011; 76:295–309.
33. Kortemme T, Ramirez-Alvarado M, Serrano L. Design of a 20-amino acid, three stranded beta sheet protein. Science. 1998; 281:253–256. [PubMed: 9657719]
34. Neidigh JW, Fesinmeyer RM, Andersen NH. Designing a 20-residue protein. Nat Struct Biol. 2002; 9(6):425–430. [PubMed: 11979279]
35. Naduthambi D, Zondlo NJ. Stereoelectronic tuning of the structure and stability of the Trp cage miniprotein. J Am Chem Soc. 2006; 128:12430–12431. [PubMed: 16984189]
36. Pastor MT, Gimenez-Giner A, Perez-Paya E. The role of an aliphatic-aromatic interaction in the stabilization of a model betahairpin peptide. Chem BioChem. 2005; 6:1753–1756.
37. Hill RB, Raleigh DP, Lombardi A, DeGrado WF. De novo design of helical bundles as models for understanding protein folding and function. Acc Chem Res. 2000; 33:745–754. [PubMed: 11087311]
38. Pantoja-Uceda D, Pastor MT, Salgado J, Pineda-Lucena A, Perez-Paya E. Design of a bivalent peptide with two independent elements of secondary strucutre able to fold autonomously. J Pept Sci. 2008; 14:845–854. [PubMed: 18247449]
39. Ben Hamidane H, He H, Tsybin OY, Emmett MR, Hendrickson CL, Marshall AG, Tsybin YO. Periodic sequence distribution of product ion abundances in electron capture dissociation of amphipathic peptides and proteins. J Am Soc Mass Spectrom. 2009; 20:1182–1192. [PubMed: 19297190]
40. Venkatachalam CM. Stereochemical criteria for polypeptides and proteins. V Conformation of a system of three linked peptide units. Biopolymers. 1968; 6:1425–1436. [PubMed: 5685102]
41. Deber CM. Evidence of β-turn analogs in proline peptides in the solid state. Infrared study. Macromolecules. 1974; 7:47–51.
42. Toniolo C. Intramolecularly hydrogen-bonded peptide conformations. CRC Crit Rev Biochem. 1980; 9:1–44. [PubMed: 6254725]
43. Hollosi M, Kawai M, Fasman GD. Studies on proline-containing tetrapeptide models of β-turns. Biopolymers. 1985; 24:211–242. [PubMed: 3886033]
44. Moehle K, Gussmann M, Hofmann H. Structural and energetic relations between β turns. J Comp Chem. 1997; 18:1415–1430.
45. Raghothama SR, Awasthi SK, Balaram P. β-Hairpin nucleation by Pro-Gly β-turns. Comparison of D-Pro-Gly and L-Pro-Gly sequences in an apolar octapeptide. J Chem Soc Perkin Trans 2: Phys Org Chem. 1998; 1:137–144.
46. Bull HB, Breese K. Surface tension of amino acid solutions: a hydrophobicity scale of the amino acid residues. Arch Biochem Biophys. 1974; 161:665–670. [PubMed: 4839053]
47. Kovacs JM, Mant CT, Hodges RS. Determination of intrinsic hydrophilicity/hydrophobicity of amino acid side chains in peptides in the absence of nearest-neighbor or conformational effects. Biopolymers. 2006; 84:283–297. [PubMed: 16315143]
48. Sibanda BL, Blundell TL, Thornton JM. Conformation of β-hairpins in protein structures. A systematic classification with applications to modeling by homology, electron density fitting, and protein engineering. J Mol Biol. 1989; 206:759–777. [PubMed: 2500530]
49. Allen SJ, Giles K, Gilbert T, Bush MF. Ion mobility mass spectrometry of peptide, protein and protein complex ions using a radio-frequency confining drift cell. Analyst. 2016; 141:884–891. [PubMed: 26739109]
50. Pringle SD, Giles K, Wildgoose JL, Williams JP, Slade SE, Thalassinos K, Bateman RH, Bowers MT, Scrivens JH. An investigation of the mobility separation of some peptide and protein ions using a new hybrid quadrupole/travelling wave IMS/oa-ToF instrument. Int J Mass Spectrom. 2007; 261:1–10.
51. Giles K, Williams JP, Campuzano I. Enhancements in traveling wave ion mobility resolution. Rapid Commun Mass Spectrom. 2011; 25:1559–1566. [PubMed: 21594930]
52. Ruotolo BT, Benesch JLP, Sandercock AM, Hyung S-J, Robinson CV. Ion mobility-mass spectrometry analysis of large protein complexes. Nat Protoc. 2008; 3:1139–1152. [PubMed: 18600219]

53. Bush MF, Hall Z, Giles K, Hoyes J, Robinson CV, Ruotolo BT. Collision cross sections of proteins and their complexes: a calibration framework and database for gas-phase structural biology. Anal Chem. 2010; 82:9557–9565. [PubMed: 20979392]
54. MacKerell AD Jr, Bashford D, Bellott M, Dunbrack RL Jr, Evanseck JD, Field MJ, Fischer S, Gao J, Guo H, Ha S, Joseph-McCarthy D, Kuchnir L, Kuczera K, Lau FTK, Mattos C, Michnick S, Ngo T, Nguyen DT, Prodhom B, Reiher WE III, Roux B, Schlenkrich M, Smith JC, Stote R, Straub J, Watanabe M, Wiorkiewicz-Kuczera J, Yin D, Karplus M. All-atom empirical potential for molecular modeling and dynamics studies of proteins. J Phys Chem B. 1998; 102:3586–3616. [PubMed: 24889800]
55. Sugita Y, Okamoto Y. Replica-exchange molecular dynamics method for protein folding. Chem Phys Lett. 1999; 314:141–151.
56. Stewart JJP. Optimization of parameters for semi-empirical methods. V Modification of NDDO approximations and application to 70 elements. J Mol Model. 2007; 13:1173–1213. [PubMed: 17828561]
57. Becke AD. New mixing of Hartree-Fock and local density-functional theories. J Chem Phys. 1993; 98:1372–1377.
58. Becke AD. Density functional thermochemistry. III The role of exact exchange. J Chem Phys. 1993; 98:5648–5652.
59. Zhao Y, Truhlar DG. The M06 suite of density functionals for main group thermochemistry, thermochemical kinetics, noncovalent interactions, excited states, and transition elements: two new functionals and systematic testing of four M06-class functionals and 12 other functionals. Theor Chem Acc. 2008; 120:215–241.
60. Møller C, Plesset MS. A note on an approximation treatment for many-electron systems. Phys Rev. 1934; 46:618–622.
61. Chai JD, Head-Gordon M. Long-range corrected hybrid density functionals with damped atom-atom dispersion corrections. Phys Chem Chem Phys. 2008; 10:6615–6620. [PubMed: 18989472]
62. Frisch, MJ.; Trucks, GW.; Schlegel, HB.; Scuseria, GE.; Robb, MA.; Cheeseman, JR.; Scalmani, G.; Barone, V.; Mennucci, B.; Petersson, GA.; Nakatsuji, H.; Caricato, M.; Li, X.; Hratchian, HP.; Izmaylov, AF.; Bloino, J.; Zheng, G.; Sonnenberg, JL.; Hada, M.; Ehara, M.; Toyota, K.; Fukuda, R.; Hasegawa, J.; Ishida, M.; Nakajima, T.; Honda, Y.; Kitao, O.; Nakai, H.; Vreven, T.; Montgomery, JA., Jr; Peralta, JE.; Ogliaro, F.; Bearpark, M.; Heyd, JJ.; Brothers, E.; Kudin, KN.; Staroverov, VN.; Kobayashi, R.; Normand, J.; Raghavachari, K.; Rendell, A.; Burant, JC.; Iyengar, SS.; Tomasi, J.; Cossi, M.; Rega, N.; Millam, JM.; Klene, M.; Knox, JE.; Cross, JB.; Bakken, V.; Adamo, C.; Jaramillo, J.; Gomperts, R.; Stratmann, RE.; Yazyev, O.; Austin, AJ.; Cammi, R.; Pomelli, C.; Ochterski, JW.; Martin, RL.; Morokuma, K.; Zakrzewski, VG.; Voth, GA.; Salvador, P.; Dannenberg, JJ.; Dapprich, S.; Daniels, AD.; Farkas, O.; Foresman, JB.; Ortiz, JV.; Cioslowski, J.; Fox, DJ. Gaussian 09, Revision A.02. Gaussian, Inc; Wallingford CT: 2009.
63. Mulliken RS. Electronic population analysis on LCAO-MO molecular wave functions. J Chem Phys. 1955; 23:1833–1840.
64. Reed AE, Weinstock RB, Weinhold F. Natural population analysis. J Chem Phys. 1985; 83:735–748.
65. Singh UC, Kollman PA. An approach to computing electrostatic charges for molecules. J Comp Chem. 1984; 5:129–160.
66. Shvartsburg AA, Jarrold MF. An exact hard-spheres scattering model for the mobilities of polyatomic ions. Chem Phys Lett. 1996; 261:86–91.
67. Mesleh MF, Hunter JM, Shvartsburg AA, Schatz GC, Jarrold MF. Structural information from ion mobility measurements: effects of the long-range potential. J Phys Chem. 1996; 100:16082–16086.
68. Campuzano I, Bush MF, Robinson CV, Beaumont C, Richardson K, Kim H, Kim HI. Structural characterization of drug-like compounds by ion mobility mass spectrometry: comparison of theoretical and experimentally derived nitrogen collision cross sections. Anal Chem. 2012; 84:1026–1033. [PubMed: 22141445]
69. Lalli PM, Corilo YE, Fasciotti M, Riccio MF, De Sa GF, Daroda RJ, Souza GHMF, McCullagh M, Bartberger MD, Eberlin MN, Campuzano IDG. Baseline resolution of isomers by traveling wave

ion mobility mass spectrometry: investigating the effects of polarizable drift gases and ionic charge distribution. J Mass Spectrom. 2013; 48:989–997. [PubMed: 24078238]

70. Chen YL, Colling BA, Douglas DJ. Collision cross sections of myoglobin and cytochrome *c* ions with Ne, Ar, and Kr. J Am Soc Mass Spectrom. 1998; 8:681–687.
71. Counterman AE, Clemmer DE. Volumes of individual amino acid residues in gas-phase peptide ions. J Am Chem Soc. 1999; 121:4031–4039.
72. Valentine SJ, Counterman AE, Clemmer DE. A Database of 660 peptide ion cross sections: use of intrinsic size parameters for bona fide predictions of cross sections. J Am Soc Mass Spectrom. 1999; 10:1188–1211. [PubMed: 10536822]
73. Lietz CB, Yu Q, Li L. Large-scale collision cross-section profiling on a traveling wave ion mobility mass spectrometer. J Am Soc Mass Spectrom. 2015; 25:2009–2019. [PubMed: 24845359]
74. Henderson SC, Li J, Counterman AE, Clemmer DE. Intrinsic size parameters for Val, Ile, Leu, Gln, Thr, Phe, and Trp residues from ion mobility measurements of polyamino acid ions. J Phys Chem B. 1999; 103:8780–8785.
75. Arunan E, Desiraju GR, Klein RA, Sadlej J, Scheiner S, Alkorta I, Clary DC, Crabtree RH, Dannenberg JJ, Hobza P, Kjaergaard HG, Legon AC, Mennucci B, Nesbitt DJ. Defining the hydrogen bond: an account. Pure Appl Chem. 2011; 83:1619–1636.
76. Hernandez PP, Maitre P, Paizs B. Zundel-type H-bonding in biomolecular ions. J Am Soc Mass Spectrom. 2014; 25:1511–1514. [PubMed: 25001386]
77. Gronert S. Determining the gas-phase properties and reactivities of multiply charged ions. J Mass Spectrom. 1999; 34:787–796. [PubMed: 10423559]
78. Gronert S. Coulomb repulsion in multiply charged ions: A computational study of the effective dielectric constants of organic spacer groups. Int J Mass Spectrom. 1999; 185/187:351–357.
79. Turecek F. Stereochemical interactions in ammonium dications. hypervalent diammonium cation radicals and ammonium radicals A B3-MP2 computational study. Eur J Mass Spectrom. 2003; 9:267–277.
80. Schnier PD, Gross DS, Williams ER. Electrostatic forces and dielectric polarizability of multiply protonated gas-phase cytochrome c ions probed by ion/molecule chemistry. J Am Chem Soc. 1995; 117:6747–6757.
81. Haeffner F, Merle JK, Irikura KK. N-protonated isomers as gateways to peptide ion fragmentation. J Am Soc Mass Spectrom. 2011; 22:2222–2231. [PubMed: 21952782]
82. Moss CL, Chung TW, Wyer JA, Nielsen SB, Hvelplund P, Tureček F. Dipole-guided electron capture causes abnormal dissociations of phosphorylated pentapeptides. J Am Soc Mass Spectrom. 2011; 22:731–751. [PubMed: 21472611]
83. von Helden G, Hsu MT, Gotts N, Bowers MT. Carbon cluster cations with up to 84 atoms: structures, formation mechanism, and reactivity. J Phys Chem. 1993; 97:8182–8192.
84. Shvartsburg AA, Mashkevich SV, Baker ES, Smith RD. Optimization of algorithms for ion mobility calculations. J Phys Chem A. 2007; 111(10):2002–2010. [PubMed: 17300182]
85. Larriba C, Hogan CJ. Ion mobilities in diatomic gases: measurement versus prediction with non-specular scattering models. J Phys Chem A. 2013; 117:3887–3901. [PubMed: 23488939]
86. Mesleh MF, Hunter JM, Shvartsburg AA, Schatz GC, Jarrold MF. Structural information from ion mobility measurements:effects of the long-range potential. J Phys Chem. 1996; 100:16082–16086.
87. Wyttenbach T, Von Helden G, Batka JJ, Carlat D, Bowers MT. Effect of the long-range potential on ion mobility measurements. J Am Soc Mass Spectrom. 1997; 8:275–282.

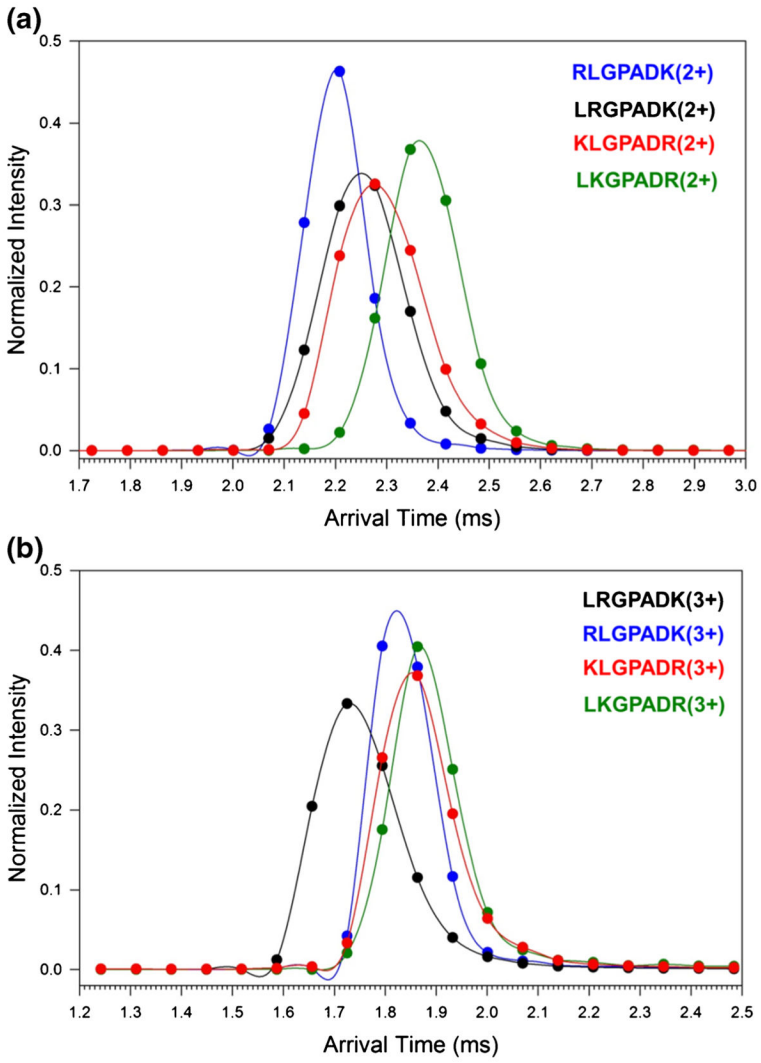

Figure 1.

Arrival time profiles in drift-cell on mobility measurements for (**a**) doubly charged and (**b**) triply charged ions

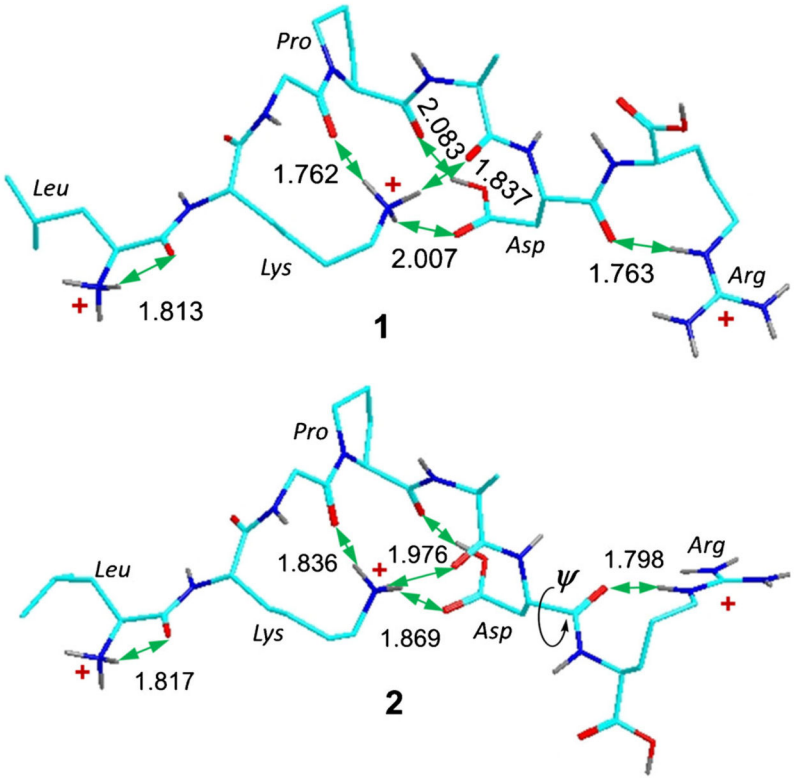

Figure 2.

B3LYP/6-31+G(d,p) optimized structures of lowest-free energy $LKGPADR^{3+}$ conformers. Atom color coding is as follows: Turquoise = C, blue = N, red = O, gray = H. Only exchangeable hydrogens in polar groups are shown. Green arrows indicate hydrogen bonds with distances given in Ångstrøms

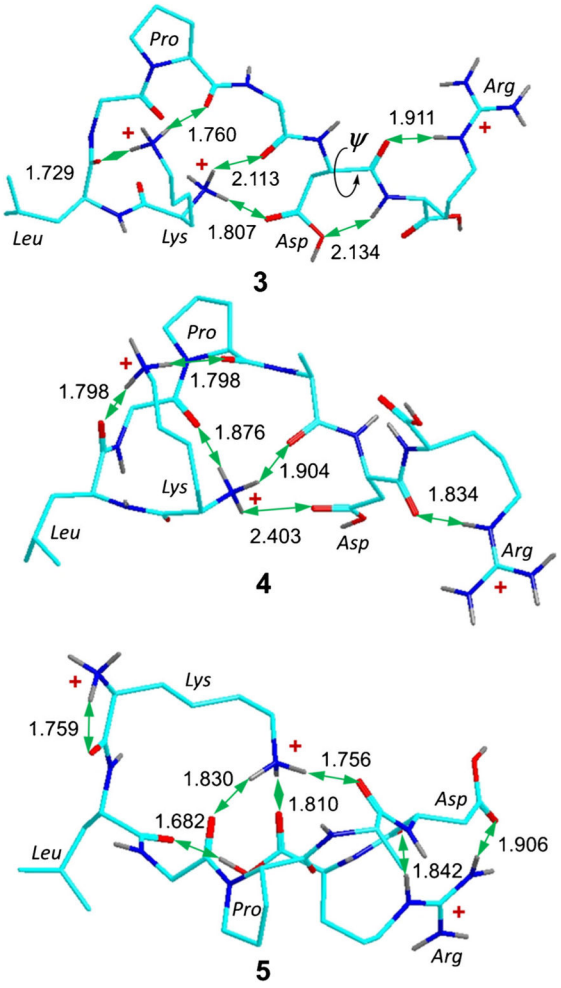

Figure 3.

B3LYP/6-31+G(d,p) optimized structures of lowest-free energy $KLGPADR^{3+}$ conformers. Structure description as in Figure 2

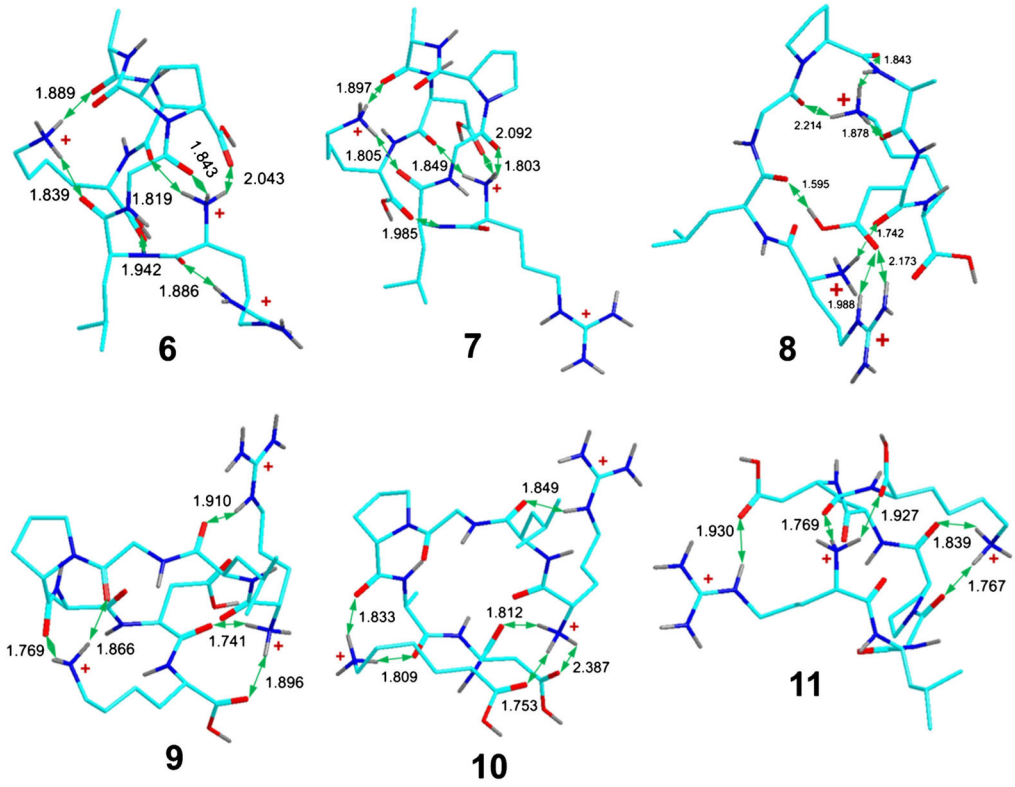

Figure 4.

B3LYP/6-31+G(d,p) optimized structures of lowest-free energy RLGPADK^{3+} conformers. Structure description as in Figure 2

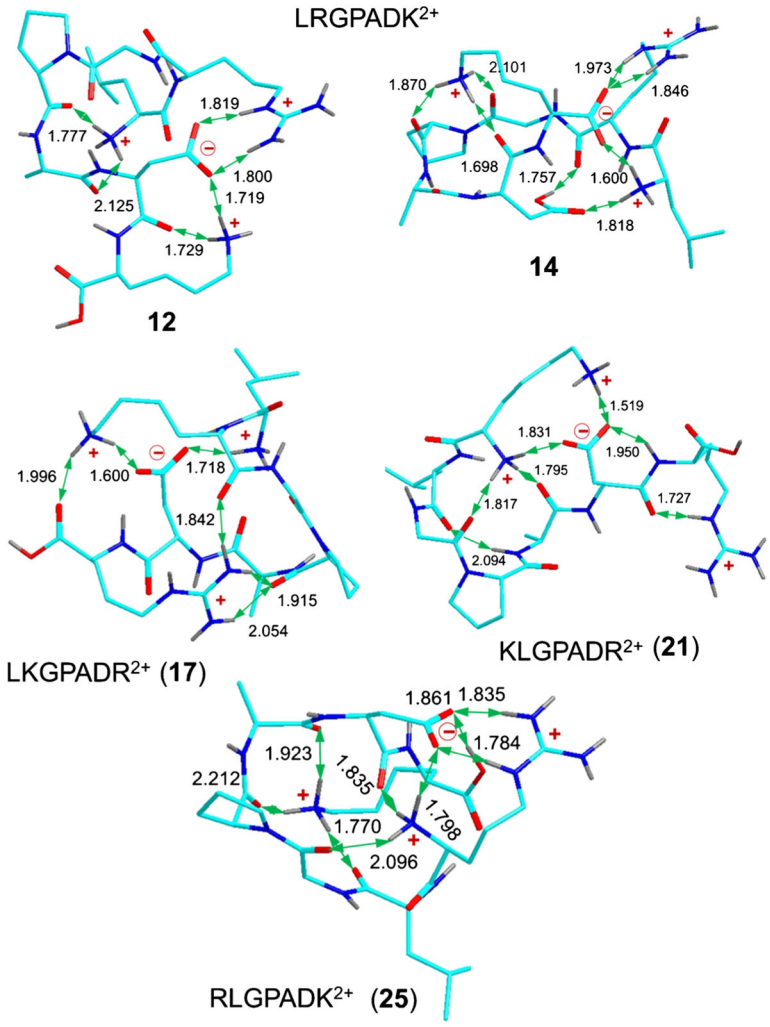

Figure 5.

B3LYP/6-31+G(d,p) optimized structures of representative lowest-free energy doubly charged ion conformers. Structure description as in Figure 2. For other structures see Supplementary Figures S2–S7 of in the Supporting Information

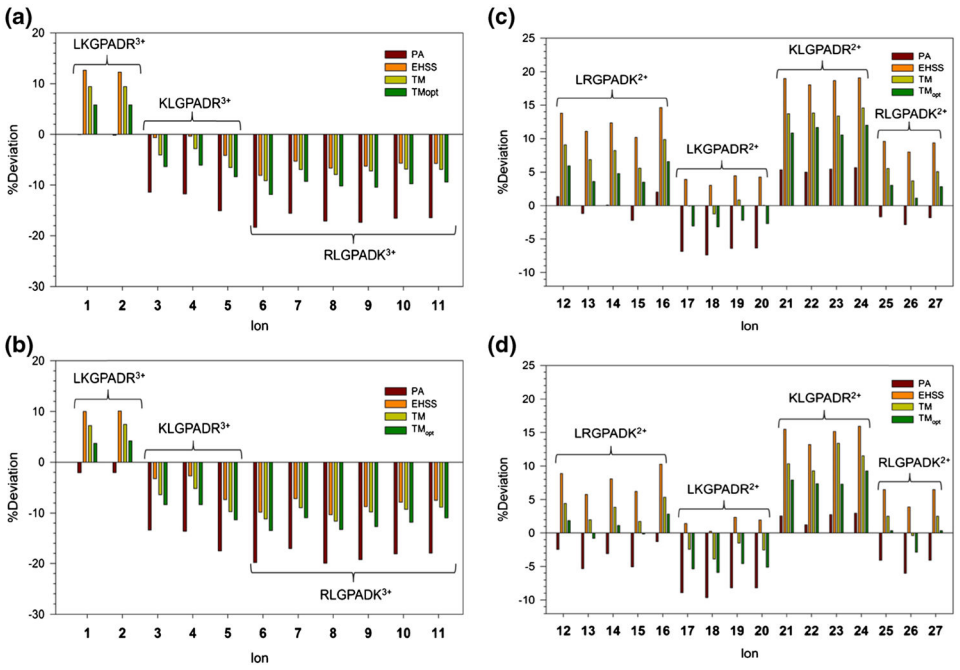

Figure 6.

Deviations of calculated collisional cross sections from experimental values for triply charged ions **1**–**11** with (**a**) B3LYP and (**b**) M06-2X optimized geometries, and doubly charged ions **12**–**27** with (**c**) B3LYP and (**d**) M06-2X optimized geometries. PA = projection average approximation, EHSS = elastic hard sphere scattering model, TM = ion trajectory model, TM_{opt} = ion trajectory with optimized parameters. See Figures 1, 2, 3, 4 and 5 and Supplementary Figures S2–S7 for optimized ion structures

Table 1

Experimental Collision Cross Sections of Peptide Ions

Peptide	Charge	Ω_{abs} (Å^2)[a]
KLGPADR	1+	185.0 ± 0.55[b]
	2+	195.4 ± 0.93
	3+	239.2 ± 4.4
LKGPADR	1+	192.6 ± 1.3
	2+	200.5 ± 1.1
	3+	226.6 ± 4.8
LRGPADK	1+	189.6 ± 0.9
	2+	192.0 ± 1.5
	3+	221.4 ± 1.3
RLGPADK	1+	188.0 ± 1.3
	2+	190.1 ± 1.3
	3+	238.3 ± 1.4

[a] From 3–4 replicate measurements on the drift-tube instrument, each based on 6–10 field-dependent arrival times with a linearity coefficient r^2 = 0.99971

[b] Standard deviations

Table 2

Relative Collision Cross Sections of Peptide Ions in Nitrogen

Peptide	Charge	$t_{d,rel}$[a]	Charge	$t_{d,rel}$[a]
KLGPADR	+2	1.00	+3	1.00
KLGPADR dimethyl ester		0.98		0.93
KLGLADR		1.04		1.01
KLGLADR dimethyl ester		1.03		0.93
LKGPADR	+2	1.00	+3	1.00
LKGPADR dimethyl ester		0.95		0.92
LKGLADR		1.02		1.02
LKGLADR dimethyl ester		1.00		0.95
LRGPADK	+2	1.00	+3	1.00
LRGPADK dimethyl ester		0.99		0.98
LRGLADK		1.03		1.03
LRGLADK dimethyl ester		1.06		1.01
RLGPADK	+2	1.00	+3	1.00
RLGPADK dimethyl ester		1.28		1.24
RLGLADK		1.03		1.01
RLGLADK dimethyl ester		1.08		0.99

[a]Relative drift times from TWIM measurements

Table 3

Calculated Relative Energies and Dipole Moments of Triply Charged Ion Conformers

Ion	Relative free energy[a]				μ(Debye)	
	B3LYP[b]	M06-2X[c]	ωB97XD[d]	MP2[b]	M06-2X	ωB97X-D
LKGPADR^{3+}						
1	0.0	0.0	0.0	0.0	12.2	12.2
2	14.0	11.7	13.8	10.5	5.1	6.6
KLGPADR^{3+}						
3	0.0	0.0	0.0	0.0	23.6	23.3
4	−7.6	−2.5	−7.5	−10.2	17.6	17.9
5	−20	6.6	−11.2	−15.1	9.5	8.9
RLGPADK^{3+}						
6	15.8	15.4	-	-	13.2	12.6
7	8.6	12.9	-	-	21.9	21.8
8	0.0	0.0	0.0	-	16.1	13.5
9	−0.9	18.9	14.4	-	4.8	5.4
10	1.4	24.1	14.1	-	9.5	10.0
11	−7.0	23.1	22.5	-	8.9	9.4

[a] In kJ mol^{-1} including zero-point energy corrections and 298 K enthalpies and entropies

[b] From single-point energy calculations with the 6-311+G(2d,p) basis set on B3LYP/6-31+G(d,p) optimized geometries

[c] From M06-2X/6-311+G(2d,p) single-point energies on M06-2X/6-31+G(d,p) optimized geometries

[d] From ωB97XD/6-311+G(2d,p) single-point energies on ωB97XD/6-31+G(d,p) optimized geometries

Table 4

Calculated Relative Energies and Dipole Moments of Doubly Charged Ion Conformers

Ion	Relative free energy[a]				μ(Debye)	
	B3LYP	M06-2X[b]	ωB97X-D[c]	MP2[d]	M06-2X	ωB97X-D
LRGPADK^{2+}						
12	0.0	0.0	0.0	0.0	10.0	10.0
13	20.3	4.5	5.7	11.1	8.0	7.9
14	12.0	2.4	11.0	28.5	6.2	6.1
15	27.0	30.5	23.5	23.9	7.6	7.9
16	1.6	3.8	6.7	7.2	11.0	11.0
LKGPADR^{2+}						
17	−0.4	2.8	4.9	5.4	4.3	5.0
18	−10.1	3.3	1.9	3.5	4.1	4.9
19	0.0	0.0	0.0	0.0	4.9	5.6
20	−9.2	2.7	0.6	3.4	4.2	4.9
KLGPADR^{2+}						
21	0.0	0.0	0.0	0.0	22.3	22.4
22	12.0	4.1	11.0	12.3	21.6	21.2
23	8.1	4.3	7.5	7.3	18.1	18.3
24	−2.3	−5.2	0	3.1	22.9	22.4
RLGPADK^{2+}						
25	0.0	0.0	0.0	0.0	7.4	7.9
26	−4.0	4.4	−3.1	−2.9	8.2	8.3
27	−0.7	−2.6	−2.8	−4.5	7.4	7.8

[a] In kJ mol^{-1} including zero-point energy corrections and 298 K enthalpies and entropies

[b] From M06-2X/6-311+G(2d,p) single-point energies on M06-2X/6-31+G(d,p) optimized geometries

[c] From ωB97X-D/6-311+G(2d,p) single-point energies on ωB97X-D/6-31+G(d,p) optimized geometries

[d] From MP2/6-311+G(2d,p) single-point energies on B3LYP/6-31+G(d,p) optimized geometries